FYSS3550

Techniques for Nuclear and Accelerator-based Physics Experiments

Home Exam

19.04.2021-30.04.2021

Jorge Romero
joromero@jyu.fi

Department of Physics

JYVÄSKYLÄN YLIOPISTO
UNIVERSITY OF JYVÄSKYLÄ

1. Lifetime measurements and Coulomb Excitation

a) To extract the lifetime of the decay from the data given on the question paper, it is necessary to plot the given normalised gamma intensity in terms of its time of flight, shown in Fig. 1.1 as red circles.

Since the recoil is moving at $v = 0.043\,\mathrm{c}$, relativistic effects can be ignored. It is possible to convert the given distances flown to times of flight by simply using $t = x/v$. With that, an intensity-time of flight plot can be drawn and fitted to an exponential decay curve of the type:

$$f(t) = a \exp\left(\frac{-t}{\tau}\right), \tag{1.1}$$

where τ is the mean lifetime and a is a constant that should be 1 when using the normalised intensities.

To account for the possibility of several decays happening for the same recoil, which are statistically more likely to be short-lived in comparison with the main decay transition, the first three points have been given a smaller weight than all other points.

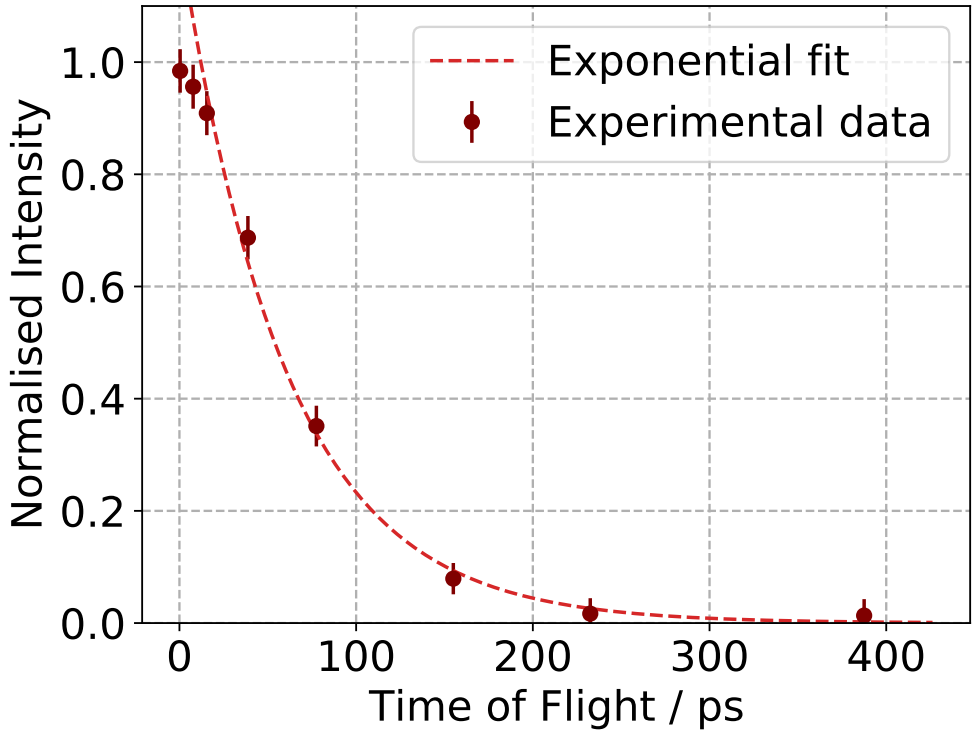

Figure 1.1: Normalised intensities as a function of time of flight. The circles are the experimental points given in the question paper and the dotted line is the exponential fit, Equation 1.1.

A different possible approach would have been to fit a convolution of several exponential decays. However, the statistical error introduced with that method would be larger than the one introduced by fitting to a single exponential.

The fitting was performed using *Python*'s package *SciPy* [1]. The mean lifetime obtained from the fit is $\tau = 60.3(36)$ ps.

b) To use the Differential Decay Curve Method (DDCM) for this data, an approximately straight section of the plot can be chosen to calculate the derivative of the curve as the slope of that straight section. The section limits are shown in Fig. 1.2 by vertical, dotted lines. The curves were extracted pointwise using *WebPlotDigitizer* [2].

The average difference between states, $\bar{\Delta}$, is 0.3, whereas the derivative is calculated pointwise as finely as possible, simply as the difference in intensity between consecutive points divided by the difference in time of consecutive points: $m_i = (y_i - y_{i-1})/(x_i - x_{i-1})$. The average of the pointwise-calculated slope is taken, $\bar{m} = \frac{1}{n}\sum_i m_i$. The DDCM mean lifetime is then estimated as:

$$\tau_{DDCM} = \frac{\bar{\Delta}}{\bar{m}} = 56(13)\,\text{ps}, \tag{1.2}$$

where the error is computed roughly as the statistical uncertainty of the averaging process.

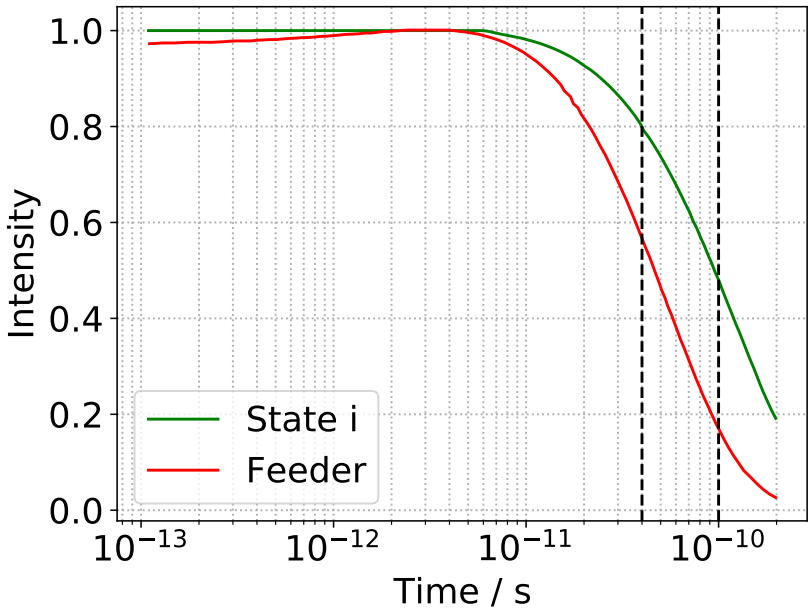

Figure 1.2: Curves shown in the question paper, with dotted lines representing the sections used as limits for the section considered for derivation.

c) Using the lifetime $\tau = (8.00 \pm 0.05)\,\text{ps}$ and the energy of the first quadrupole state of ^{208}Rn (2^+, 635.8 keV) [3], it is possible to extract the B(E2) of its decay by rearranging the equation for the lifetime of a generic EL transition:

$$\left(\frac{1}{\tau}\right)_{EL} = \frac{8\pi(L+1)\,\text{e}^2\text{b}^L}{L[(2L+1)!!]^2\hbar}\left(\frac{E_\gamma}{\hbar c}\right)^{2L+1} B(EL), \tag{1.3}$$

where the values $E_\gamma = 635.8\,\text{keV}$, $\tau = 8\,\text{ps}$ and $L = 2$ can be substituted to obtain $B(E2) = 0.0982\,\text{e}^2\text{b}^2$. $B(EL; I_i \to I_f)$ can be related to the transition matrix elements by:

$$B(EL; I_i \to I_f) = \frac{1}{2I_i + 1}||\mathcal{M}_{if}||^2, \tag{1.4}$$

therefore, matrix element 0,2 can be obtained as:

$$\mathcal{M}_{02} = \sqrt{5 \times 0.0982\,\text{e}^2\text{b}^2} = 0.701(2)\,\text{eb}. \tag{1.5}$$

In the χ^2 graph, this corresponds to values of $\mathcal{M}_{22}$ comprised between -1.0 and 0.3. The quadrupole moment, Q_0 can be calculated from $\mathcal{M}_{22}$ as:

$$Q_0 = \sqrt{\frac{16\pi}{5}}\mathcal{M}_{22}, \tag{1.6}$$

giving $Q_0(max) = 0.951\,\text{eb}$ and $Q_0(min) = -3.17\,\text{eb}$. This therefore results in a calculated value of $\boxed{Q_0 = -1.11(206)\,\text{eb}}$.

2. Recoil separators, reactions, energy losses

a) To select the appropriate beam and target combination to use to produce ^{120}La in MARA, firstly, we need to determine what the possible beam compositions are. For that, we can visit the ECR Beam Database [4] of the University of Jyväskylä's Ion Source Group.

To produce ^{120}La through fusion-evaporation, a suitable compound nucleus has to be produced, which will be more massive than ^{120}La. Candidates include ^{122}Ce (decaying to ^{120}La through the pn channel), ^{123}Ce (p2n channel), ^{124}Pr (2p2n channel), and other isotopes of lanthanum with a higher A, decaying through the xn channel, where x is A-120.

To produce a compound in this region, a target of mass around A=65 is needed, with a beam of mass around A=60. By analysing the possible beams in [4] and the corresponding targets, with the condition that the target material should be a stable nucleus, the following reaction is chosen: a $^{58}_{28}\mathrm{Ni}_{30}$ beam impinging on a $^{66}_{30}\mathrm{Zn}_{36}$ target. This produces a compound nucleus of $^{124}_{58}\mathrm{Ce}^*_{76}$, which then can decay through the p3n channel to produce ^{120}La.

$$^{66}\mathrm{Zn} + {}^{58}\mathrm{Ni} \rightarrow {}^{124}\mathrm{Ce}^* \rightarrow {}^{120}\mathrm{La} + p + 3n. \tag{2.1}$$

The reaction of ^{58}Ni onto ^{63}Cu to produce ^{121}La* and evaporate one proton was also considered, but the fusion cross section was too low for the energies in which only one proton would be evaporated, making it almost impossible to get to ^{120}La with this particular reaction.

b) To calculate the required bombarding energy, the separation energies of the intermediate nuclei have to be taken into account, to calculate the excitation energy, E^*, of the compound nucleus. These energies are shown in Table 2.1:

Table 2.1: Relevant separation energies for the compound nucleus and intermediate nuclei [5].

Nucleus	S_n [MeV]	S_p [MeV]
^{124}Ce	-	0.269
^{123}La	12.179	-
^{122}La	10.424	-
^{121}La	12.692	-
Total	35.295	0.269

The energies in Table 2.1 amount to a total separation energy of 35.564 MeV. In addtion, an average of 3 MeV of kinetic energy per emitted particle has to be taken into account. Since 4 nucleons will be emitted, 12 MeV have to be added, obtaining an excitation energy of $E^* = 47.6$ MeV.

It is now necessary to calculate the reaction Q-value, from their mass excess. The fusion Q-value will be:

$$Q_{fus} = -\Delta M(\text{compound}) + \Delta M(\text{target}) + \Delta M(\text{beam}), \tag{2.2}$$

where ΔM represents the mass excess. Table 2.2 shows the mass excess for each of these nuclei according to [5].

Table 2.2: Mass excess for the nuclei involved in the reaction in Equation 2.1 [5].

Nucleus	ΔM [MeV]
^{124}Ce	-64.916
^{66}Zn	-68.899
^{58}Ni	-60.229

The reaction Q-value, calculated using Equation 2.2, is $Q_{fus} = -64.212\,\text{MeV}$. Since the centre-of-mass energy is given by $E_{CM} = E^* - Q$, for this reaction $E_{CM} = 111.8\,\text{MeV}$. By a simple conversion:

$$E_{lab} \approx \frac{A_A + A_B}{A_A} E_{CM} \Rightarrow E_{lab} = \frac{66+58}{66} \times 111.8 = 210.1\,\text{MeV}. \tag{2.3}$$

Calculating the Coulomb barrier energy as:

$$V_C = \frac{Z_1 Z_2}{A_1^{1/3} + A_2^{1/3}} = \frac{28 \cdot 30}{58^{1/3} + 66^{1/3}} = 106.2\,\text{MeV}, \tag{2.4}$$

we can see that the reaction is well above the Coulomb barrier, and therefore can occur.

The energy at the middle of the target (MOT) will be 210 MeV. Since the target is assumed to be $0.7\,\text{mg/cm}^2$, this means that the bombarding energy has to jjjj such that the remaining energy after $0.35\,\text{mg/cm}^2$ of target is 210 MeV. From SRIM [6], we can obtain the stopping power of ^{58}Ni in ^{66}Zn, which is $20.71\,\text{MeV/(mg/cm}^2)$ at 225 MeV beam energy. With this in mind, the energy loss in half of the target's thickness will be:

$$20.71\,\text{MeV/(mg/cm}^2) \times 0.35\,\text{mg/cm}^2 = 7.25\,\text{MeV},$$

making it so that the optimal bombarding energy is **217.25 MeV**. This was also verified with the LISE++ code [7].

c) To calculate the magnetic field and electric potential needed for ^{120}La's transport through MARA, it is necessary to obtain its kinetic energy after the target. It is possible to calculate its energy at the middle of the target, T_{MOT}, thanks to the conservation of angular momentum, as:

$$T_{MOT} = E_{lab} \cdot \frac{A_{beam}}{A_{comp}} \cdot \frac{A_{recoil}}{A_{comp}} = 210\,\text{MeV}\frac{58 \cdot 120}{124^2} = 95\,\text{MeV}. \tag{2.5}$$

After this, the stopping power of ^{120}La in ^{66}Zn is needed, as this is the MOT energy. The recoils will still need to go through $0.35\,\text{mg/cm}^2$ of target. Additionally, MARA has a thin, $20\,\mu\text{g/cm}^2$ carbon foil after the target position, which the recoil will also need to traverse.

The stopping power of ^{120}La in ^{66}Zn at 95 MeV is $28\,\text{MeV/(mg/cm}^2)$. Thus, after $0.35\,\text{mg/cm}^2$, the recoils would have deposited 10 MeV and be left with 85 MeV.

The stopping power of ^{120}La in $^{\text{nat}}$C at 85 MeV is $57\,\text{MeV/(mg/cm}^2)$. The thickness of the C foil is $0.02\,\text{mg/cm}^2$, so the recoil will deposit 1.1 MeV and therefore leave with a final kinetic energy of $T = 83.9\,\text{MeV}$.

It is now possible to calculate the recoil velocity from its kinetic energy, as:

$$T = \frac{1}{2}mv^2 \Longrightarrow v = \sqrt{\frac{2T}{m}}. \tag{2.6}$$

In this case, with the recoil's mass being $m = 120\,\text{u}$, it is possible to obtain the velocity in terms of the speed of light as:

$$v = \sqrt{\frac{2 \cdot 83.9\,\text{MeV}}{120\,\text{u} \cdot 931.5\,\text{MeV/(uc}^2)}} = 0.0387\,\text{c}. \tag{2.7}$$

Which can be used to calculate the reduced speed with $v' = 0.012\,\text{c}$ [8]:

$$x = \frac{v}{v' + Z^{0.45}} = 0.523, \tag{2.8}$$

which serves to estimate the average charge state in which the recoils will leave. This will be calculated as [8]:

$$\bar{q} = Z\left[1 + x^{-1/0.6}\right]^{-0.6} = 25. \tag{2.9}$$

Also from [8], we can find the distribution of charge states as:

$$d_{\bar{q}} = \frac{1}{2}\sqrt{\bar{q}\left[1 - \left(\frac{\bar{q}}{Z}\right)^{1/0.6}\right]} = 2.16 \to 2, \tag{2.10}$$

which means that, although charge state 25 is the average and more commonly produced, charge states 24 and 26 will also be produced.

Having this, the values for the deflector electric potential, V, and the magnetic dipole field, B, for MARA to focus this charge state to the centre of the focal plane will be:

$$V = \frac{T}{q} \ln\left(\frac{R_2}{R_1}\right), \tag{2.11}$$

$$B = \frac{\sqrt{2mT}}{q\rho_B}, \tag{2.12}$$

where T is the alpha energy in MeV, m is the mass of the recoil in u (120 in this case), q is the charge of the particle (25 in this case), $\rho_B = 1\,\text{m}$ is the magnetic radius and R_2 and R_1 are the outer and inner electrode radii, respectively, where, since MARA has a symmetric setup, $R_{\frac{1}{2}} = \rho_E \mp 0.07$, as the half-radius of the deflector is subtracted or added to the electric radius, $\rho_E = 4\,\text{m}$ [9].

Solving these equations with the derived and given values, the resulting MARA optical tuning parameters to have the possible charge states centred at the focal plane are shown in Table 2.3.

Table 2.3: MARA Optical Parameters for ^{120}La at 83.9 MeV and relevant charge states.

Charge State	V[V]	B[T]
24	122 367	0.602
25	117 472	0.578
26	112 954	0.556

d) By calculating the values of m/q for the three relevant charge states shown in the previous section (q = 24,25,26), and using $m = 120$, it can be seen in Table 2.4, a one unit charge state difference with respect to $q = 25$ results in a $\sim 4\%$ change in m/q.

Table 2.4: ^{120}La m/q values for relevant charge states and their percentage difference with respect to $\bar{q} = 25$.

Charge State	m/q	$\Delta(m/q)$ [%]
24	5.000	+4.17
25	4.800	0.00
26	4.615	-3.85

Due to this, and considering the 8.00 mm/(% m/q), charge states will be separated by 32 mm at the MWPC. Since the MWPC is 128 mm wide, with charge state 25 centred at its middle, there are 64 mm available at each side of the central

charge state. Therefore, 2 additional charge states can fit the MWPC on each side of the central one, although the ones on the extremes may lose some counts if not very well focused. Therefore, we can say that we would expect **5 charge states within the MWPC** under ideal conditions.

e) Firstly, to calculate the angular cone, it is necessary to identify the three angular components of the recoils:

1. Multiple scattering in the target foil, $\alpha_{1/2}^{scatt}$,
2. Angular component due to particle emission, $\alpha_{1/2}^{part}$,
3. Beam emittance from the cyclotron, $\alpha_{1/2}^{beam}$.

The beam emittance from the cyclotron is fixed at $\alpha_{1/2}^{beam} = 5\,\text{mrad}$, so only the other two components need to be calculated.

For the first one, it is necessary to calculate the reduced angles:

$$\begin{aligned}\tilde{\alpha} &= \frac{aE_p}{Z_pZ_t(Z_p^{2/3}+Z_t^{2/3})^{1/2}}\alpha,\\ \tilde{\alpha}_{1/2} &\approx 0.25\tau,\\ \tau &= \frac{41.5\rho}{A_t(Z_p^{2/3}+Z_t^{2/3})},\end{aligned}$$

where $a = 0.885a_0\left(Z_p^{2/3}+Z_t^{2/3}\right)^{-1/2}$, a_0 is Bohr's radius, ρ is the thickness of the target and t and p in subscripts represent target and projectile, respectively.

Combining all of these, we can arrive at:

$$\alpha_{1/2}^{scatt} = \frac{11.723\cdot Z_pZ_t\rho}{a_0E_pA_t}. \tag{2.13}$$

The projectile energy is $T_{MOT} = 95\,\text{MeV}$, as calculated in Equation 2.5. In total, this amounts to $\alpha_{\mathbf{1/2}}^{\mathbf{scatt}} = \mathbf{13.8\,mrad}$.

The angular component due to particle emission, $\alpha_{1/2}^{part}$, is defined as:

$$\alpha_{1/2}^{part} = \frac{2.36}{2}\sigma = \frac{2.36}{2}\sqrt{\Omega_n}, \tag{2.14}$$

where

$$\Omega_n = \sum_i \frac{p_i^2}{3p_{comp}^2}. \tag{2.15}$$

p_i and p_{comp} are the momenta of the emitted neutrons and the compound nucleus, respectively. Since $p^2 = \sqrt{2Em}$, and all 4 emitted particles are emitted with 3 MeV and have the same mass ($m_p \approx m_n$), Equation 2.15 can be rewritten as:

$$\Omega_n = \frac{4 \times 3\,\text{MeV} \times 1\,\text{u}}{3 \times 98.2\,\text{MeV} \times 124\,\text{u}}, \tag{2.16}$$

due to $E_{comp} = \frac{A_{beam}}{A_{comp}} E_{lab} = \frac{58}{124} \times 210\,\text{MeV} = 98.2\,\text{MeV}$. In total, substituting Equation 2.16 into 2.14, we obtain the final angular component due to particle emission, $\alpha_{\mathbf{1/2}}^{\mathbf{part}} = \mathbf{21.48\,mrad}$.

Combining all of these, the total angular cone turns out to be:

$$\boxed{\alpha_{1/2} = \sqrt{13.8^2 + 21.4^2 + 5^2} = 26\,\text{mrad}.} \tag{2.17}$$

The angular acceptance of MARA is ±50 mrad when considering both x and y directions, so the entire cone will be accepted.

Finally, to calculate the energy straggling, it is necessary to calculate the individual components of energy straggling. These are:

i. Beam energy distribution. This is calculated as $\Delta E_{beam} = 0.01 E_{beam}$, in this case, $\Delta E_{beam} = 2.1\,\text{MeV}$.

ii. Broadening due to thickness, calculated as:

$$\Delta E_{thick} = \left| \delta E_{rec} + \delta E_{beam} \frac{A_{beam}}{A_{rec}} \right|. \tag{2.18}$$

In this case, $\delta E_{beam} = 14.5\,\text{MeV}$ and $\delta E_{rec} = 10\,\text{MeV}$, so $\Delta E_{thick} = 17\,\text{MeV}$.

iii. Broadening due to straggling in the target foil, calculated as:

$$\Delta E_{strag} = 2.89{\times}10^{-2} \left[\delta E_{beam} Z_{beam} Z_t \left(Z_{beam}^{1/3} + Z_t^{1/3} \right)^{-2} + \delta E_{rec} Z_{rec} Z_t \left(Z_{rec}^{1/3} + Z_t^{1/3} \right)^{-2} \right]^{1/2}. \tag{2.19}$$

In total, when substituting in, the result is $\Delta E_{strag} = 1.25\,\text{MeV}$.

iv. Broadening due to particle emission, calculated as:

$$\Delta E_{part} = \frac{2\sqrt{8 \ln 2}}{\sqrt{3}} \sqrt{\bar{E}_{rec} \frac{\bar{E}_n}{A_{rec}}}, \tag{2.20}$$

where $\bar{E}_n$ and $\bar{E}_{rec}$ are the average energies for the nucleons emitted and the recoil, respectively. $\bar{E}_n = 3\,\text{MeV}$ and $\bar{E}_{rec}$ can be calculated as:

$$\bar{E}_{rec} = (A_{beam} \frac{A_{rec}}{A_{comp}^2})(E_{beam} - 0.5\delta E_{beam}) - 0.5\delta E_{rec}. \tag{2.21}$$

In this case, $\bar{E}_{rec} = 99.4\,\text{MeV}$ and thus, $\Delta E_{part} = 7.4\,\text{MeV}$.

In total now, we can calculate the total energy straggling:

$$2\delta_T = \sqrt{\Delta E_{beam}^2 + \Delta E_{thick}^2 + \Delta E_{strag}^2 + \Delta E_{part}^2} = 18.7\,\text{MeV} \Rightarrow \boxed{\delta_T = 9.4\,\text{MeV}.} \tag{2.22}$$

Since the emerging kinetic energy is 83.9 MeV, this δ_T is 11%. Since MARA's energy acceptance is 20%, this recoil will be entirely accepted.

3. Separation of Masses

To speak about static electric and magnetic fields, it is convenient to first introduce the **Lorentz Force**:

$$\vec{F} = q\left(\vec{E} + \vec{v} \times \vec{B}\right), \tag{3.1}$$

which describes the force experienced by a particle of charge q due to an electric ($\vec{E}$) and/or a magnetic ($\vec{B}$) field, when moving through them with velocity $\vec{v}$.

The first term in this force, $q\vec{E}$, is known as the electric force, which is the force that a particle feels only due to its interaction with an electric field. If the electric field is not time-dependent, it is said to be static. Therefore, the electric force felt by the particle is an **electrostatic force**. From Newton's second law, which can be written as $\vec{F} = m\vec{a}$, we know that a net force on a particle will consitute an acceleration which will be proportional to the magnitude of said force and inversely proportional to the mass of that particle. Considering only static electic fields, the acceleration of a particle of charge q and mass m is:

$$\vec{a} = \frac{q}{m}\vec{E}. \tag{3.2}$$

It is therefore possible to study the mass of a particle by the use of electrostatic fields by meausring its acceleration when its charge and the applied electric field is known:

$$m = \frac{qE}{a}, \tag{3.3}$$

where now only the magnitudes of the vectors are taken because the acceleration and electrostatic fields are parallel. If this is applied for a radial field, charged particles will feel a centripetal force towards the source of the field, of the form $F_c = ma_c = \frac{mv^2}{r}$, where r is the radius of the trajectory of the particles and v their velocity. In the absence of other forces, the centripetal acceleration will also be the net acceleration, thus $a = a_c = \frac{v^2}{r}$ and therefore, combining this with Equation 3.3:

$$m = \frac{qr}{v^2}E. \tag{3.4}$$

The resolving power of this technique is only dependent on the precision of the electric field applied, as the charge will remain constant, and radius and velocity are dependent upon the electrostatic field.

An example of this being used for research is in MARA's electrostatic deflector [9], at the University of Jyväskylä. Here, due to the use of two electrodes, the equation is slightly different:

$$V = \frac{mv^2}{2q}\ln\left(\frac{R_2}{R_1}\right) \Rightarrow m = \frac{2qE}{v^2\ln\left(\frac{R_2}{R_1}\right)}, \tag{3.5}$$

where R_i are the radii of curvature of the outer and inner electrodes. v is only dependent on the energy the recoils are emitted from the target foil at, and q is the charge at which they exit. Thus, only E affects resolution here. Fig. 3.1 shows how mass resolution is affected in MARA by small changes in E differently depending on the original voltage around which the fluctuation happens. As can be seen in the figure, a bigger electrostatic field is less sensitive to fluctuations in terms of mass resolution.

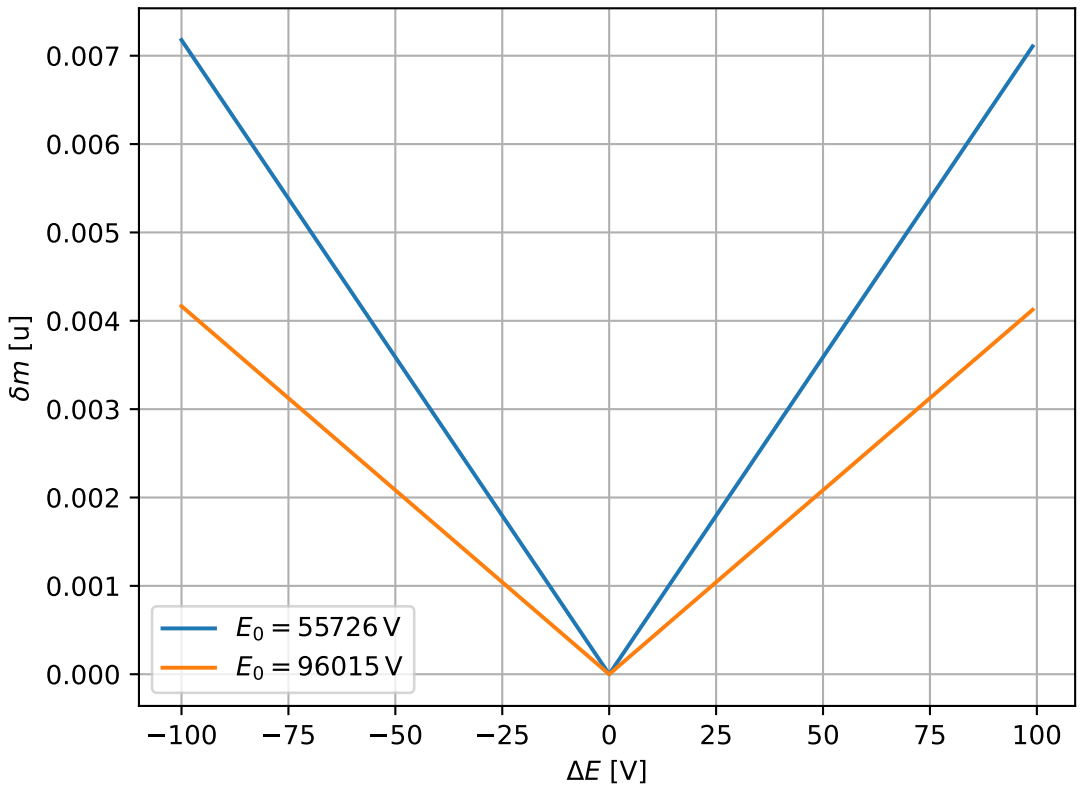

Figure 3.1: Difference in mass resolution δm with respect to the original mass in terms of variations around the optimal field in MARA's electrostatic deflector. Calulated for two alpha particles of different energy and thus different optimal electric field E_0.

If, instead of an electrostatic field, a static magnetic field is used, the second term of the Lorentz force (Equation 3.1) comes into play. The **magnetic force**, $\vec{F} = q(\vec{v} \times \vec{B})$, is the force felt by a charged particle of charge q that traverses a static magnetic field $\vec{B}$ at velocity $\vec{v}$. Due to the cross-product, the resulting force is perpendicular both to the magnetic field and the direction of motion. This results in circular paths and therefore a centripetal force. In absence of other

forces, this results in:

$$F_c = F_B, \tag{3.6}$$

$$\frac{mv^2}{r} = qvB, \tag{3.7}$$

$$m = \frac{qr}{v}B. \tag{3.8}$$

Similarly to the electrostatic case, the charge, radius and velocity are fixed for a particle coming into the magnetic field. Thus, only the field strength is relevant. In the case of MARA's dipole magnet [9], the dipole radius is $\rho_B = 1\,\mathrm{m}$. Since the charge state and speed will be fixed, again there will be a linear dependance between mass resolution and B. This will be accentuated at lower B values, as the percentage difference will be higher for the same change around the optimal setting, and a similar shape to that shown in Fig. 3.1 will be seen.

A different way of measuring the mass of a particle is the **Time of Flight** technique. This technique is based on the fact that applying a force on a particle will result on an acceleration which is inversely proportional to that particle's mass. This is a consequence of Newton's second law, $\vec{F} = m\vec{a}$.

When not under any force, a particle's velocity will be simply defined as the distance it is able to traverse in a certain amount of time, $v = \frac{\mathrm{d}x}{\mathrm{d}t}$. Therefore, if one can measure the time it takes for a particle to traverse a distance after having been accelerated, its mass can be determined as follows:

A particle can be accelerated by a known force which will result in a uniform acceleration $a = F/m$ for a time t_a. The acceleration is then stopped, leaving the particle at a constant velocity: $v = \frac{F}{m}t_a$. The particle's linear velocity can be measured in the time interval t_a to t_f by the distance x covered by the particle in that time $v = \frac{x}{t_f - t_a}$, thus arriving at:

$$\frac{F}{m}t_a = \frac{x}{t_f - t_a},$$

thus, the mass of the particle can be obtained as:

$$m = \frac{Ft_a}{x}(t_f - t_a) = \frac{Ft_a}{x}\Delta t. \tag{3.9}$$

Since F, the applied force, t_a, the time during which the force is applied, and x, the distance that the particle is left unaccelerated before being mesured, are fixed values, the mass resolution is only dependant on the precision of the measurement of Δt, the time of flight of the particle.

Since the mass resolution is dependent on this time of flight, and a longer time of flight will result in less loss in resolution for a variation in time of flight,

some techniques aim to maximise the time of flight to minimise the loss in mass resolution. One such techinique is the **Multi-Reflection Time of Flight** (MR-TOF). This technique is based on the reflection of charged particles via electric and magnetic fields, in order to have them traverse a long distance (thus longer ToF), but while confined in a physically small space.

Radio-Frequency Quadrupoles (RFQ) use alternating electric fields, at varying frequencies, to trap particles within a confined space. Particles inside an RFQ experience a force upon them [10]:

$$m\frac{\mathrm{d}^2x}{\mathrm{d}t^2} = \frac{-2q}{r_0^2}\left[U + V\cos\left(2\pi ft\right)\right]x, \tag{3.10}$$

in a similar manner to other techniques, the only variable on which mass resolution depends is frequency, f. In this case, U and V are also dependent on f. The optimal frequencies for this techinque, as its name points at, are the Radio-Frequencies, from around 20 kHz to about 300 GHz. This is because the dependence with frequency in this case is not linear, unlike in the other cases presented, which means that an optimal point must be reached to optimise for mass resolution.

A combination of the former and a strong, static magnetic field is the **Penning trap**. These traps use quadrupole electric fields for axial confinement and a strong magnetic field in the axial direction for radial confinement [11]. In this case, like with RFQs, there are specific frequencies that are of importance in mass analysis using these traps. Mass resolution is very high with the use of Penning traps, and the precision on frequency has to be very well known for accuracy in the mass measurements. Both RFQs and Penning traps are used at IGISOL, in the Univerisity of Jyväskylä.

4. Radiation Effects

The plot shows the Single-Event-Upset (SEU) cross section for two devices in terms of the Linear Energy Transfer (LET) value of particles traversing the device.

LET is a measure of the amount of energy deposited by an ionising particle when passing through a material. This depends on both the particle and the material, in addition to depending on the energy of the particle. In general, particles which are more energetic will produce fewer ionisations due to them having a shorter interaction time with the material. The opposite is true for less energetic particles. However, for very low energies, the particle may completely stop and not cause ionisations.

In the case of memory devices, where information is stored in bits, which depend on the electronic state of a component and are binary in nature, an ionisation can "flip" a bit, making it go from one binary state to the other, completely altering the stored data.

These curves show the cross section of these bit-flipping events on each device in terms of the LET of the ionising particle that may cause it.

Device 1 has a higher SEU cross-section for higher LET values than Device 2, but falls quicker to 0 when reducing LET. This means that for higher LET values, Device 1 will suffer more SEU than Device 2. However, for smaller values of LET (LET $\lesssim 9\,\mathrm{MeV/(mg/cm^2)}$), Device 1 has a lower SEU cross-section (less likelihood of corruption) than Device 2. In fact, the SEU cross-section for Device 1 falls to 0 at around $5\,\mathrm{MeV/(mg/cm^2)}$, whereas this happens to Device 2 at around $1\,\mathrm{MeV/(mg/cm^2)}$. This shows that for LET values of 0-5 $\mathrm{MeV/(mg/cm^2)}$, Device 2 will get SEU events, but not Device 1. This is what makes Device 1 more suitable for LEO satellites, because particles cosmic radiation reaching Low-Earth Orbit is more likely to have smaller LET values [12], thus making it valuable to have a small SEU cross-section for those than for high-LET particles.

Taking Device 1 now, and assuming a substrate layer of 70 µm of Si and a fluence of $10^7\,\mathrm{ions/cm^2}$, we can calculate what the energy of the Kr ions is after passing through the substrate. Using LISE++ [7], it is possible to compute the energy loss of a ^{82}Kr beam at 768 MeV in silicon. LISE++ integrates the path of the beam using the values tabulated in SRIM [6]. With this, the energy loss is 593 MeV after 70 µm of Si substrate. Therefore, 175 MeV remain when arriving at the memory.

Now, the LET of ^{82}Kr in Si at 175 MeV has to be obtained. This can also be taken from SRIM by considering that LET $\approx \frac{\mathrm{d}E}{\mathrm{d}x}$ for Kr. The LET of ^{82}Kr in Si at 175 MeV according to SRIM is $40.89\,\mathrm{MeV/(mg/cm^2)}$.

Now, it is only necessary to use:

$$\sigma_{SEU} = \frac{N_{err}}{\Phi_{ion} N_{bit}} \tag{4.1}$$

to estimate the number of errors in the die. Reading from the given graph that the SEU cross-section for 41 MeV/(mg/cm^2)is $\sigma_{SEU} = 2.5 \times 10^{-11}$ cm^2/bit and knowing that the memory contains 2048^3 bits, it is then easy to calculate the expected number of errors:

$$N_{err} = \sigma_{SEU} \cdot \Phi_{ion} \cdot N_{bit} = 2.5 \times 10^{-11}\,\text{cm}^2/\text{bit} \times 10^7\,\text{ions/cm}^2 \times 2048^3\,\text{bits} = 2.15 \times 10^6.$$

If the substrate had a variation of ±30 µm from the thickness stated before, it would affect the number of errors, as it will affect the LET of the Kr beam when reaching the memory. Repeating the calculations done before, but for a 40 µm- and a 100 µm-thick substrate, the Kr beam energies after the substrate are:

$$\begin{aligned} \text{E}(40\,\mu\text{m}) &= 453.6\,\text{MeV}, \\ \text{E}(100\,\mu\text{m}) &= 0\,\text{MeV}. \end{aligned}$$

The beam will not penetrate the 100 µm-thick substrate, as its range at 768 MeV is 93.8 µm. Plotting the LET values obtained from SRIM for this energy range, we obtain the curve shown in Fig. 4.1. In the figure, it can be seen that the maximum value of LET is around the one obtained for the nominal thickness of 70 µm, which corresponds to around 41 MeV/(mg/cm^2). From the graph given in the question, we can see that all LET values under 41 MeV/(mg/cm^2) correspond to SEU cross-sections smaller than that of 41 MeV/(mg/cm^2).

This means that the maximum SEU cross-section happens for a thickness of 70 µm, and having different thicknesses in the given range only decreases this cross-section. Therefore, the number of expected errors should decrease if that much variation is present in the substrate thickness.

For energies over around 175 MeV, where the maximum LET happens, LET only varies by around 5 units. This decrease will only vary the cross-section within the same order of magnitude, therefore not affecting the final number of errors by much. However, for lower energies (thicker substrates), the LET drops rapidly. It is only below a LET of 10 MeV/(mg/cm^2), however, that the change in cross section spans a different order of magnitude. This will happen only for the thickest of substrates, at thicknesses over 90 µm.

Assuming a uniform distribution of imperfections from 40 to 100 µm, thicknesses of 90 µm or more will correspond to 16.7% of the surface of the substrate. Due to the rapid fall of the cross-section below this, and the fact that energies over 10 MeV will correspond to approximately the same SEU cross-section, we can say that the number of errors expected when this imperfect thinning is considered will be 83.3% of that obtained with a properly performed thinning, therefore:

$$\boxed{N'_{err} \approx 0.833 N_{err} = 1.79 \times 10^6}$$

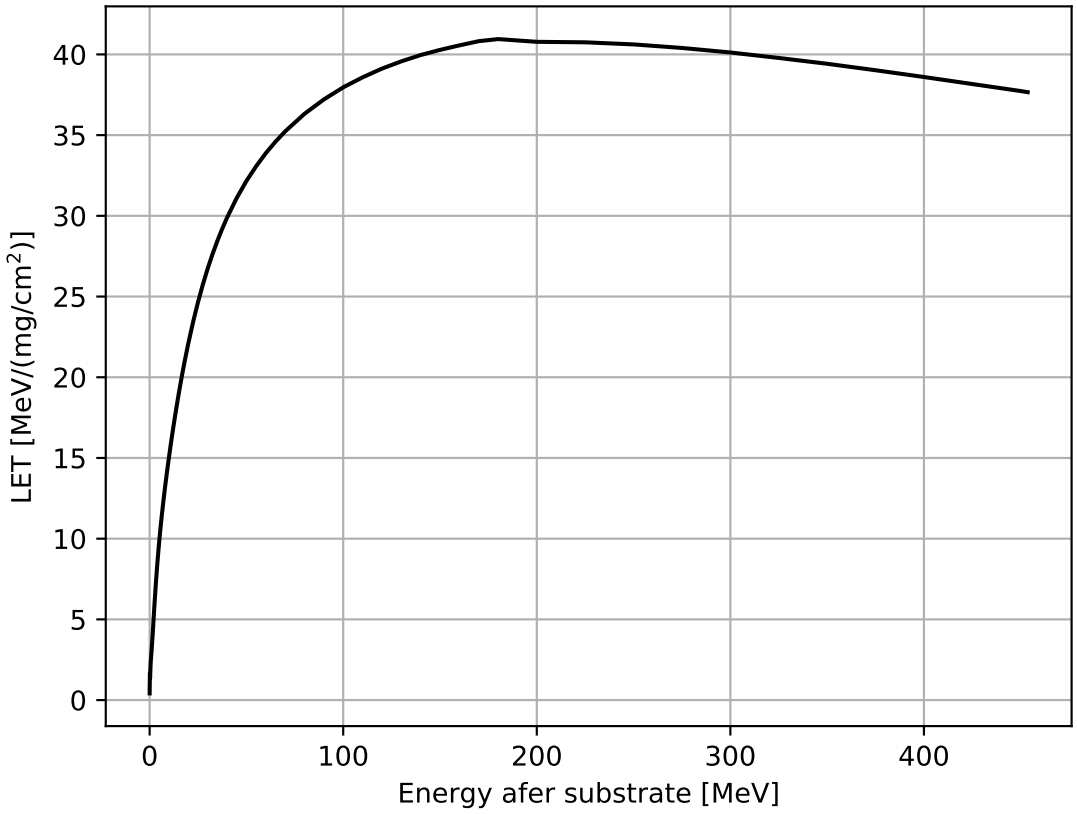

Figure 4.1: LET values for ^{82}Kr impinging on Si for different energy values, corresponding to a range of substrate thicknesses from 40 to 100 µm. Values taken from SRIM [6].

5. Ion Beam Analysis

a) To identify the unkown elemental compostitions of the film, substrate and beam, the *Potku* [13]. By plotting the Energy as a function of Time-of-Flight (ToF), several elemental traces are visually apparent. It is possible to add 2D gates to delimit the edges of the traces in *Potku*. The program can then perform a calibration if the gates and beam are labeled correctly.

For this, a preliminary analysis of the shape of the plot has to be done. A hypothesis of the compositions can be developed from that. If the hypothesis is correct, the calibration will be linear and all point will lie on the calibration line.

For the initial hypothesis, the strongest traces can be identified as the film. Since the only possible film compositions are Al_2O_3 and AlN, we know that the more massive of these traces has to correspond to aluminium. By knowing that more massive atoms have a longer ToF, we can identify the strong trace on the right (the trace that has the highest energies) as the aluminium trace. All traces to the left of this one correspond to atoms which are lighter than it.

There is only one trace to the right of this one, and the bottom of the trace is thicker, which indicates that there is an unresolved second trace next to it. Since a substrate candidate is silicon, the neighbouring element to aluminium, we can take it for the preliminary hypothesis, ruling out germanium.

There is still a heavier atom than aluminium and silicon in the spectrum, so fluorine can be ruled out as a beam component. Due to the distance to the last trace, we can take the heaviest possible beam component, Cu, for the hypothesis.

Finally, the traces to the left of the aluminium-tagged one have to be identified. Due to the structure seen, and knowing that the only candidates for these are nitrogen and oxygen as part of the film, the three-trace structure reveals that this must be nitrogen with some carbon and oxygen contamination. If the central, strong trace were oxygen, the slightly higher mass trace would have to be fluorine or neon contamination, which is unlikely.

Therefore, the discussed traces are identified as such in *Potku*, with the areas shown in Fig. 5.1 as discussed. The resulting calibration plot is shown in Fig. 5.2. It can be seen in this figure that the calibration points shown for the hyposethised atoms with Cu as a beam lie on the calibration line. It can therefore be confirmed that they were correctly selected.

The setup is, therefore, as follows:

- Beam: ^{63}Cu
- Substrate: Si
- Foil: AlN

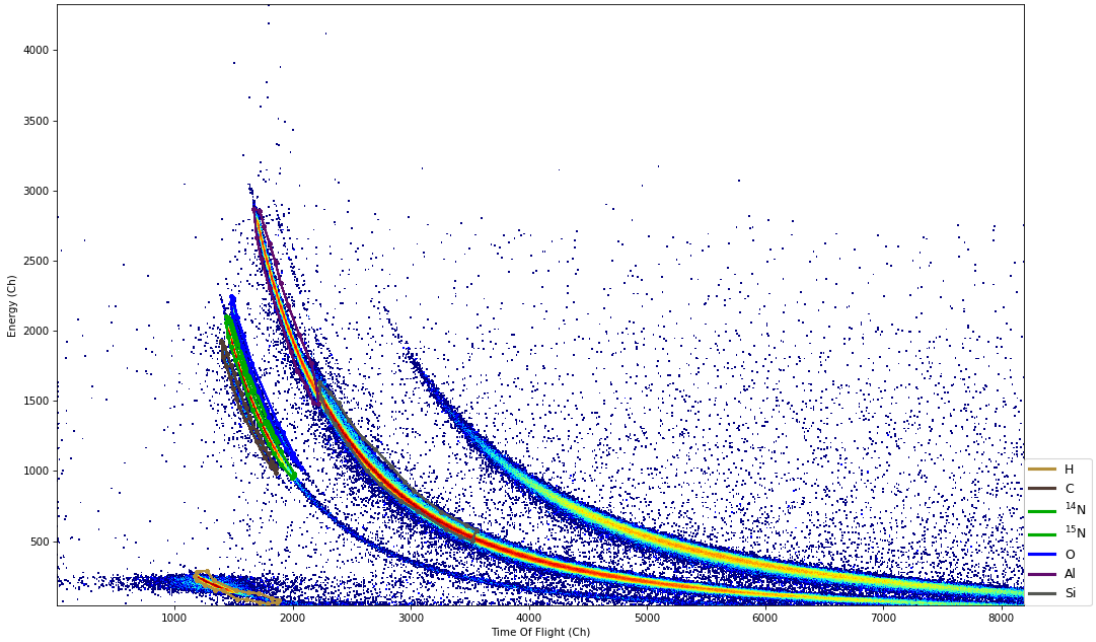

Figure 5.1: Energy to Time of Flight diagram for the whole dataset, including gates for several elemental traces.

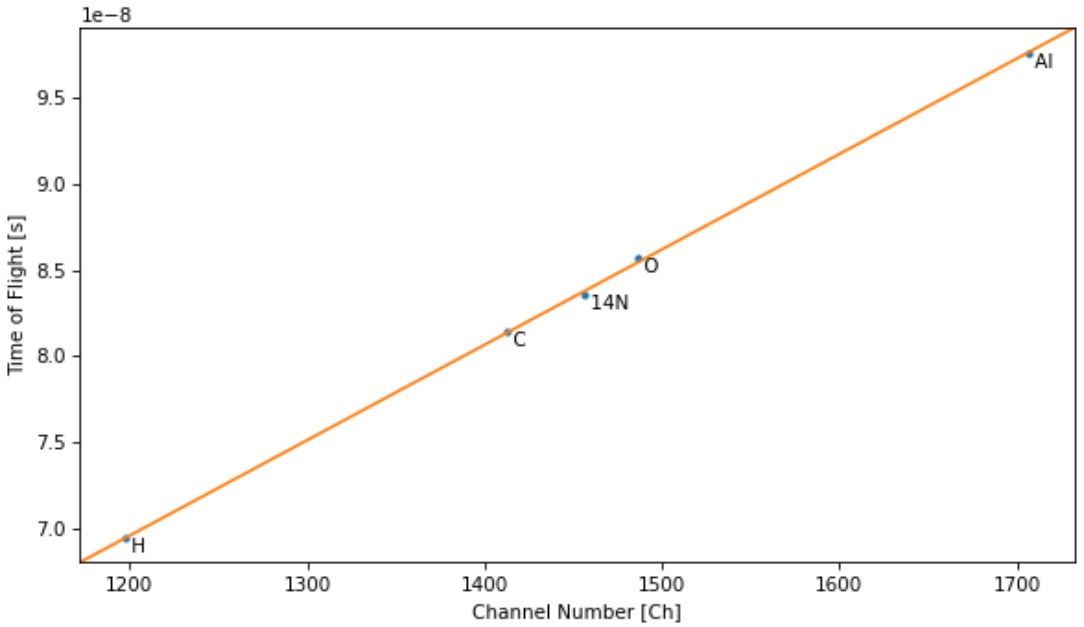

Figure 5.2: Linear calibration performed by Potku, all points being on the line indicate that the elemental traces were tagged correctly.

b)

References

[1] P. Virtanen, et al., Nat. Meth. 17 (2020) 261.

[2] A. Rohatgi, Webplotdigitizer: Version 4.4 (2020).
URL https://automeris.io/WebPlotDigitizer

[3] M. Martin, Nucl. Data Sheets 108 (2007) 1583.

[4] H. Koivisto, et al., ECR beam database, http://users.jyu.fi/~japelaul/ecr_beam_database/toe.php.

[5] W. J. Huang, et al., Chinese Phys. C 45 (2021) 030002.

[6] J. F. Ziegler, Stopping and range of ions in matter, www.srim.org.

[7] NSCL/MSU, Lise++ code, http://lise.nscl.msu.edu/lise.html.

[8] V. S. Nikolaev, I. S. Dmitrev, Phys. Lett. A 28 (1984) 277.

[9] J. Sarén, The ion-optical design of the mara recoil separator and absolute transmission measurements of the ritu gas-filled recoil separator, Ph.D. thesis, University of Jyväskylä (2011).

[10] R. E. March, J. Mass Spect. 32 (1997) 351.

[11] L. Brown, G. Gabrielse, Rev. Modern Phys. 58 (1986) 233.

[12] A. B. Akopova, et al., Int. J. Radiat. Appl. Instrum. D 17 (1990) 93.

[13] JYU-IBA, Potku, analysis software for tof-erda with integrated mcerd, https://www.jyu.fi/science/en/physics/research/infrastructures/accelerator-laboratory/pelletron/potku.